

Scanning coherent x-ray microscopy as a tool for XFEL nanobeam characterization

Andreas Schropp^{a,c}, Robert Hoppe^a, Jens Patommel^a, Frank Seiboth^a, Fredrik Uhlén^b, Ulrich Vogt^b, Hae Ja Lee^c, Bob Nagler^c, Eric C. Galtier^c, Ulf Zastra^c, Brice Arnold^c, Philip Heimann^c, Jerome B. Hastings^c, and Christian G. Schroer^a

^aInstitute of Structural Physics, Technische Universität Dresden, D-01062 Dresden, Germany

^bBiomedical & X-Ray Physics, KTH/Royal Institute of Technology,

AlbaNova University Center, SE-106 91, Stockholm, Sweden

^cSLAC National Accelerator Laboratory, 2575 Sand Hill Road, Menlo Park, CA 94025, USA

ABSTRACT

During the last years, scanning coherent x-ray microscopy, also called ptychography, has revolutionized nanobeam characterization at third generation x-ray sources. The method yields the complete information on the complex valued, nanofocused wave field with high spatial resolution. In an experiment carried out at the Matter in Extreme Conditions (MEC) instrument at the Linac Coherent Light Source (LCLS) we successfully applied the method to an attenuated nanofocused XFEL beam with a size of 180(h) × 150(v) nm² (FWHM) in horizontal (h) and vertical direction (v), respectively. It was created by a set of 20 beryllium compound refractive lenses (Be-CRLs). By using a fast detector (CSPAD) to record the diffraction patterns and a fast implementation of the phase retrieval code running on a graphics processing unit (GPU), the applicability of the method as a real-time XFEL nanobeam diagnostic is highlighted.

Keywords: x-ray optics, compound refractive lenses, ptychography, coherent x-ray imaging, x-ray free electron laser

1. INTRODUCTION

The emergence of x-ray sources of the fourth generation, so called x-ray free-electron laser (XFELs), comes along with completely new research opportunities in various scientific fields.¹⁻⁴ In some experiments, however, the XFEL beam needs to be additionally focused in order to increase the fluence incident on a sample. A detailed characterization of nanofocused x-ray beams is important in various experimental scenarios where the quantitative analysis requires the knowledge of the two-dimensional intensity distribution hitting a sample rather than an integral dose. This concerns scientific areas like coherent x-ray imaging,² high-energy density physics,³ or nonlinear optics.⁴ Nevertheless, since the peak intensity of these focused beams is well above the damage threshold of any material, the characterization of a nanofocused XFEL beam is experimentally challenging and, to date, was pursued primarily by imprint techniques providing only *postmortem* information of the intensity distribution.⁵

Scanning coherent x-ray microscopy, often also named ptychography, is a relatively recent imaging technique. Although the scheme was already proposed by Hegerl and Hoppe for applications in electron microscopy in 1970,⁶ it took more than 30 years to be rediscovered by Rodenburg and Faulkner in 2004.^{7,8} The method is based on the scanning of a sample through a coherent and spatially confined x-ray beam and the recording of a far-field diffraction pattern at each position of the scan. In the case that there is a sufficiently large amount of overlap between adjacent illuminated areas, numerical algorithms exist that are able to retrieve a high resolution image of the sample and refine the complex valued illumination function at the same time.⁹⁻¹² The method provides the complete information on the x-ray wave field illuminating the sample, which is especially interesting in the case that the x-ray beam was focused by x-ray optics in order to increase the fluence on a sample.¹³⁻¹⁵ In this

Correspondence: A. Schropp. E-mail: schropp@xray-lens.de

way, important information on the performance of the x-ray optics used for nanofocusing is obtained, which largely facilitates the development of improved x-ray optics.¹⁶

In this proceedings paper we summarize experimental developments carried out at the Matter in Extreme Conditions (MEC) instrument of the Linac Coherent Light Source (LCLS) in order to fast and routinely characterize nanofocused x-ray free-electron laser (XFEL) beams using ptychography. By implementing fast pixel detectors such as the Cornell-SLAC pixel array detector (CSPAD)^{17,18} and fast numerical phase retrieval routines running on GPUs, a real-time characterization of XFEL nanobeams is within reach.

2. SCANNING COHERENT X-RAY MICROSCOPY – PTYCHOGRAPHY

Lensless coherent x-ray imaging is a relatively recent microscopy technique, which has strongly developed during the last decade.¹⁹ It allows one to obtain structural information of objects with a spatial resolution ultimately only limited by the wavelength λ of the radiation and the number of photons available during an experiment.^{20,21} By positioning a sample of size D in a coherent x-ray beam, a continuous diffraction pattern can be measured in forward direction showing speckles with a characteristic minimum angular size of $\theta = \lambda/D$. In order to be able to retrieve structural information from this far-field diffraction pattern, these speckles must be resolved by the detector. Given a detector with pixel size p and positioned at a distance L from the sample, the Shannon sampling demands a minimum angular resolving power of the detector given by $p/L < \theta/2$, or $p < \lambda L/(2D)$. If this sampling condition is fulfilled the real space structure can be retrieved from the diffraction pattern using phase retrieval methods.²² The applicability of the method was demonstrated in various experiments^{23–25} and could be extended to the imaging of three-dimensional structures.^{26,27} By applying it in Bragg-angle geometry, information on strain fields within nanocrystals can be obtained.²⁸ However, main limitations of the method are the requirement that only objects of finite size D , limited by the sampling requirements given above, can be investigated and phase retrieval algorithms often suffer from the so-called twin image problem. The latter refers to the existence of multiple solutions for a single diffraction pattern like the true structure, its complex conjugate or the point reflected structure. Therefore, the iterative phase retrieval algorithm often converged slowly or got even trapped in local minima of the optimization problem.

In 2004, Rodenburg and Faulkner suggested a method, so called ptychography, which is a hybrid of lensless coherent x-ray imaging and scanning microscopy.^{7,8} The method is based on the scanning of a sample through a spatially confined and coherent x-ray beam. At each scan position a far-field diffraction pattern is recorded. Instead of requiring objects of limited extension, the size of the illuminating wave field has to be small enough to fulfill the sampling requirements in reciprocal space, which can be achieved either by using small pinholes or by focusing the x-ray beam. It was first demonstrated by Schroer, *et al.*, in 2008 that the coherence properties of a focused x-ray beam are preserved as long as the optic is coherently illuminated.²⁹ In this way, extended objects can be investigated and the previously mentioned sampling requirement of coherent lensless x-ray imaging is transferred to an illumination of confined size. Additionally, by choosing the size of the scanning steps such as to guarantee some overlap between neighboring scan points,¹⁰ stagnation difficulties of phase retrieval algorithms can be avoided and fast phase retrieval algorithms are available. The measurement of multiple diffraction patterns is related to a certain degree of overdetermination of the inversion problem containing enough information to retrieve not only high resolution information on the object²¹ but also on the complex valued illumination function at the same time.¹² As a side product ptychography revolutionized nanobeam characterization at third generation x-ray sources.^{13,14,16} Recently, the method was extended to accommodate additionally the use of partially coherent illuminating wave fields.³⁰ In the following, the ptychographic phase retrieval algorithm as proposed by Maiden, *et al.*, will be described.³¹

The phase retrieval algorithm starts with a guess of a complex valued transmission function of the object $O(\mathbf{r})$ and the complex valued illumination function $P(\mathbf{r})$. Typically, we define an object with unit transmission and set the illumination function to a real-valued Gaussian intensity distribution. Since the object is scanned through the x-ray beam, different areas of the object are illuminated and translational displacements are identified by the vector \mathbf{r}_j (cf. Fig. 1). The complex multiplication of illumination and object function yields a representation of the wave field $\psi_j(\mathbf{r})$ behind the object at a certain scan point j . It is then propagated to the reciprocal space by applying the Fourier transform, $\tilde{\psi}_j(\mathbf{q}) = \mathcal{F}[\psi_j(\mathbf{r})]$. Then, amplitudes are replaced by the measured values $\sqrt{I_j(\mathbf{q})}$ while keeping the phases $\phi_j(\mathbf{q})$ unchanged. By propagating the wave field back to real space,

$\mathcal{F}^{-1}[\tilde{\psi}_j(\mathbf{q})]$, a new guess $\psi'_j(\mathbf{r})$ is obtained, and an updated illumination and object function are extracted from $\psi'_j(\mathbf{r})$ by applying effectively a deconvolution scheme:³¹

$$P'(\mathbf{r}) = P(\mathbf{r}) + \alpha \frac{O^*(\mathbf{r} - \mathbf{r}_j)}{|O(\mathbf{r} - \mathbf{r}_j)|_{\max}^2} (\psi'_j(\mathbf{r}) - \psi_j(\mathbf{r})), \text{ and} \quad (1)$$

$$O'(\mathbf{r} - \mathbf{r}_j) = O(\mathbf{r} - \mathbf{r}_j) + \beta \frac{P^*(\mathbf{r})}{|P(\mathbf{r})|_{\max}^2} (\psi'_j(\mathbf{r}) - \psi_j(\mathbf{r})), \quad (2)$$

where P^* and O^* refer to the complex conjugates of illumination and object function, and α and β are real valued constants.

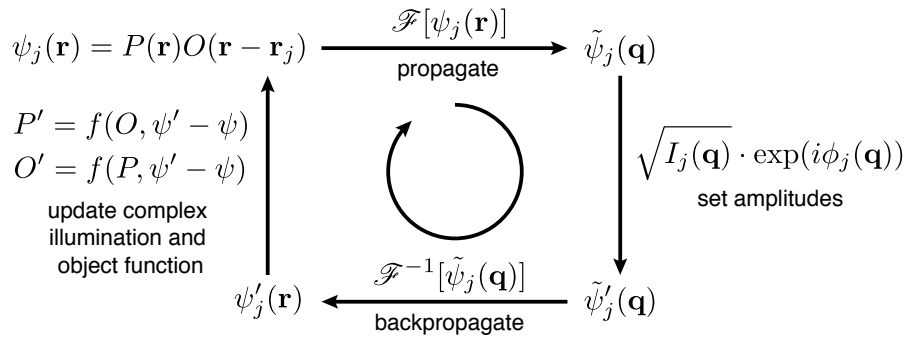


Figure 1. Schematic of the Ptychographic phase retrieval algorithm.

We call one iteration completed after applying this scheme to all diffraction patterns j . Typically, convergence is achieved after a few iterations for the complex illumination function. Depending on the accuracy of the position data \mathbf{r}_j , the convergence of the transmission function is slower and requires a few tens to a few hundreds of iterations.

3. NANOFOCUSING SETUP

The MEC instrument at the LCLS is located at the very end of the facility in the far-experimental hall (FEH) and provides the experimental environment required for high pressure, density and temperature experiments. A large vacuum chamber with a diameter of 2 m in the center of the hutch constitutes the main experimental area and provides enough space to implement the focusing setup based on refractive x-ray optics. The vacuum chamber is positioned at a distance of 464 m from the source. Since the SASE XFEL beam has a bandwidth of approximately $\Delta E/E = 0.2\%$, a four bounce, Barthels-type, Si(111) monochromator (K-mono) had to be used to guarantee the necessary temporal coherence. It is located at a distance of 87.6 m from the source and reduces the bandwidth of the XFEL beam to $\Delta E/E = 1.5 \cdot 10^{-4}$. Approximately 1% of the full SASE XFEL beam is transmitted by the monochromator. The XFEL beam intensity was further attenuated by polished single crystal silicon absorbers such as to prevent the saturation of the detector.

In Fig. 2 an overview of the experimental setup at MEC is presented. A set of 20 parabolically shaped compound refractive x-ray lenses made of beryllium (Be-CRLs) was integrated into the chamber in order to focus the LCLS-beam to a theoretical beam size of approximately 115 nm at a focal distance of 250 mm behind the optic [cf. Fig. 2 b) and Fig. 2 c)]. Since Ptychography is based on the measurement of far-field diffraction patterns, the distance between the sample and the detector has to be sufficiently large to fulfill the sampling requirements. In this case, the setup was extended by a 3 m-long, evacuated tube, which was attached to the main chamber and was sealed at its other end with a Kapton window [cf. Fig. 2 a)]. Further downstream and outside vacuum two detectors (CSPAD-140k and Rayonix SX165) were installed to measure the diffraction patterns [cf. Fig. 2 d)]. The sample used for Ptychography was mounted on top of a PI Nanocube P-615 which operates with a positioning repeatability of better than 10 nm [cf. Fig. 2 c)].

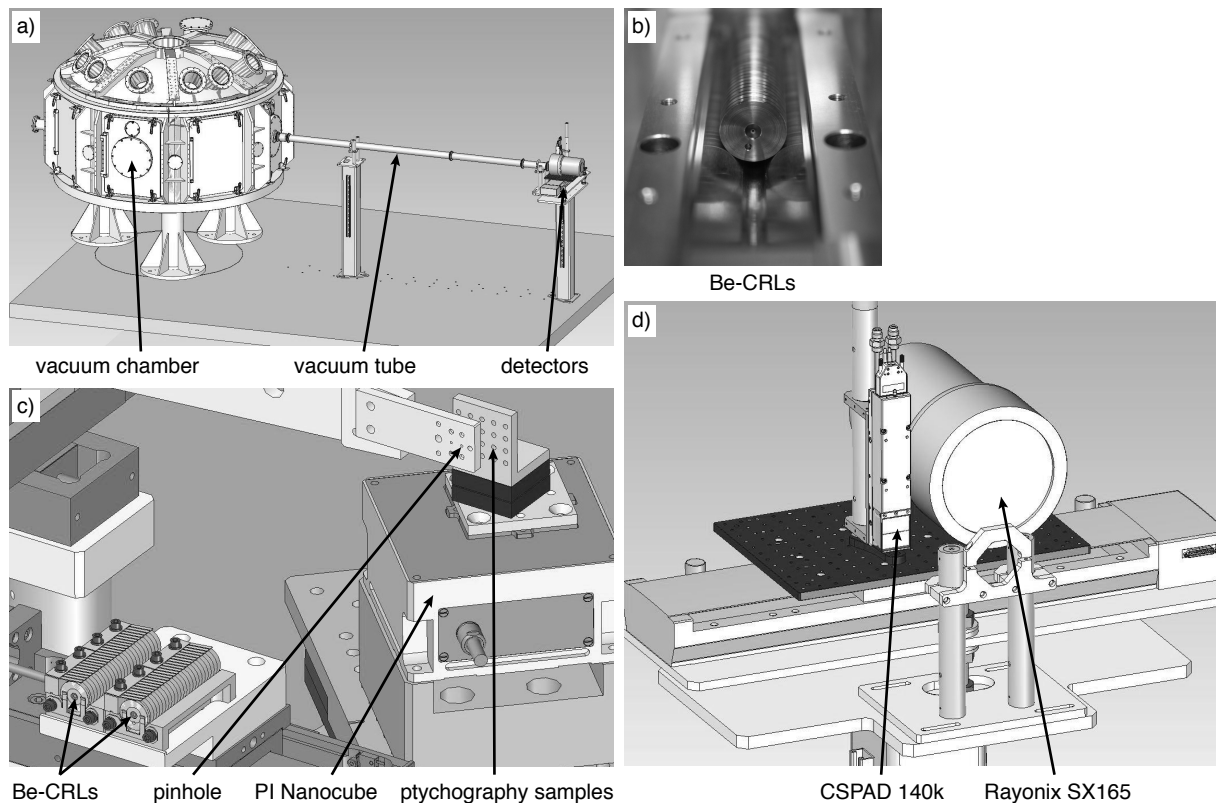


Figure 2. a) MEC vacuum chamber extended by an evacuated tube and showing the detector-mount. b) Beryllium compound refractive lenses (Be-CRLs). c) Optical setup inside the chamber showing the Be-CRLs and the pinhole (diameter of $30\ \mu\text{m}$). The latter was used to clean the nanofocused XFEL beam from background scattering. The sample was positioned with a PI Nanocube (P-615). d) Detectors that were mounted outside vacuum.

4. XFEL NANOBEAM CHARACTERIZATION

The ptychographic measurement was carried out on a $1\ \mu\text{m}$ -thick tungsten nano-structure containing an array of 40 by 40 identical Siemens stars. A single Siemens star has a size of approximately $2\ \mu\text{m}$ and contains smallest features with a size of $50\ \text{nm}$. The tungsten layer was sputter deposited onto a $100\ \mu\text{m}$ -thick CVD diamond substrate. A quadratic area of the sample with a size of $1\ \mu\text{m}^2$ was scanned with the nanofocused XFEL beam on a grid with $20(\text{h}) \times 200(\text{v})$ scan points and a step size of $50\ \text{nm}(\text{h})$ and $5\ \text{nm}(\text{v})$ in horizontal and vertical direction, respectively. In total, 4000 diffraction patterns were recorded from an area of $1\ \mu\text{m}^2$ in less than one minute. The best 322 diffraction patterns having a large diffraction signal were used for the ptychographic reconstruction.

We used a CSPAD-140k detector for this experiment which allows one to record diffraction patterns at a frame rate of 120 Hz. Therefore, the sample could be scanned continuously in the vertical direction and was not halted at individual scan positions. In this direction the Nanocube piezomotor was driven at constant speed of $600\ \text{nm/s}$ while the LCLS was operating continuously at 120 Hz. At this speed the sample moves only by a distance of $3 \cdot 10^{-20}\ \text{m}$ during an individual XFEL pulse of 50 fs time duration, which is far negligible as compared to other positioning errors related to instabilities of the setup or drifting stages. In horizontal direction the sample was scanned in discrete steps of $50\ \text{nm}$.

The CSPAD-140k has an area of 391×397 pixels with a pixel size of $p = 110\ \mu\text{m}$. It was positioned at a distance of $L = 4.14\ \text{m}$ behind the sample. For the reconstruction a sub-array of $N^2 = 256 \times 256$ pixels was used, which yields at the photon energy of $8.2\ \text{keV}$ ($\lambda = 1.51\ \text{\AA}$) a pixel size in the reconstructed image of $\Delta x = \lambda L / (Np) = 22.2\ \text{nm}$. In Figs. 3 a) – 3 d) a selection of measured diffraction patterns is shown. Due to a

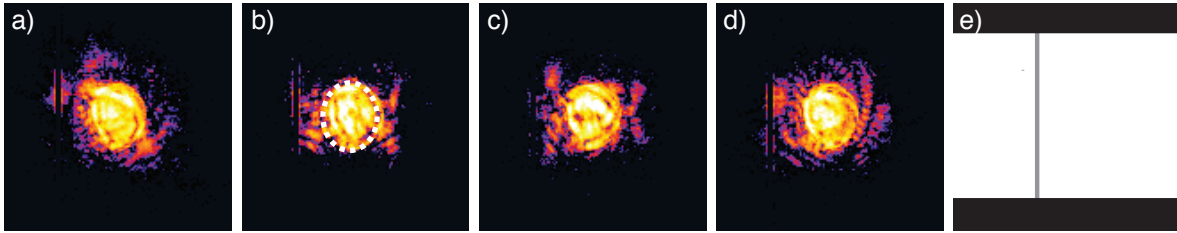


Figure 3. a) – d) Selection of diffraction patterns measured with the CSPAD-140k. Due to a slight tilt of the Be-CRLs in the horizontal plane, the central intensity peak has a rather oval than the expected circular shape as indicated by a white dotted line in image b). e) Mask used during the reconstruction in order to identify pixels of the detector which contain a spurious diffraction signal. Black areas were set to zero during the iterative phase retrieval process, and light gray pixels were not constrained and could freely evolve. Only diffraction data measured in the white regions were used for the phase retrieval.

slight tilt of the Be-CRLs in the horizontal plane the central intensity peak appears rather oval than circular as indicated by a white dotted line in Fig. 3 b). This small misalignment leads finally to an additional aberration of the optic and increases effectively the size of the focus. In Fig. 3 e) the mask is shown that was applied during the iterative phase retrieval in order to identify either insensitive areas of the detector or other bad pixels. Black assigns areas where the amplitude of the scattered wave field was set to zero in each iteration. Regions colored in light gray were not constrained and could freely evolve, and in white zones the amplitude was set to the measured values. Additionally, since the convergence of the object's transmission function depends sensitively on the knowledge of the correct position values, these values were refined every 50 iterations. The refinement procedure is based on a local search using the current guess of illumination and object function. In this case, for each measured diffraction pattern an area of 5×5 pixels around the theoretical position was searched by evaluating the least square difference between the simulated and the measured diffraction pattern. Further detailed information on the position refinement procedure can be found elsewhere.³²

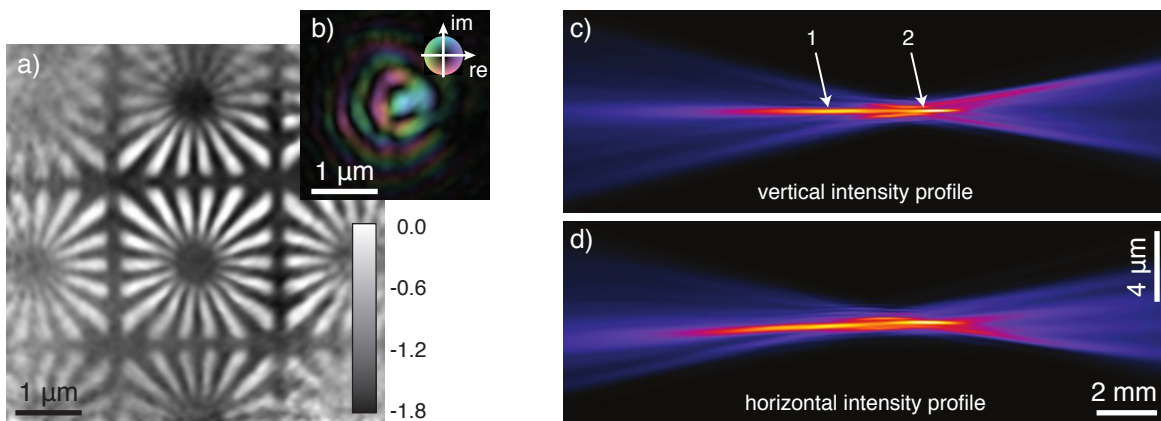


Figure 4. a) Reconstructed phase of the transmission function of the object. b) Reconstructed complex illumination function. The phase is encoded by color as indicated in the inset. c), d) Vertical and horizontal intensity profile, respectively.

In Fig. 4 a) the reconstructed image of the object after 1000 iterations is shown. Gray values refer to the phase shift in radian (see inset). The maximum phase shift in the reconstructed image is $\varphi_{\max} = -1.8$ rad, which is in a very good agreement to the theoretical value of $\varphi_W = -k\delta_W d = -1.87$ rad for a $1 \mu\text{m}$ thick tungsten layer. Here, the wave number $k = 2\pi/\lambda = 4.15 \cdot 10^{10} \text{ m}^{-1}$, the refractive index decrement $\delta_W = 4.5 \cdot 10^{-5}$ (photon energy of $E = 8.2 \text{ keV}$) and the thickness of the tungsten layer $d = 1 \mu\text{m}$ were used. In Fig. 4 b) the reconstructed illumination function in the plane of the object after 1000 iterations is presented. The phase is encoded by color

as indicated by the color wheel in the inset and the amplitude by brightness. Once the complex illumination function in a plane perpendicular to the x-ray beam is known, the wave field can be numerically propagated along the optical axis yielding the complete information on the focused XFEL nanobeam. In Fig. 4 c) and 4 d) the integrated intensity distribution in vertical and horizontal direction is shown, respectively.

The intensity distribution in the vertical direction shows the known performance of the Be-CRLs having a slight spherical aberration.³² As a result of this aberration rays that are close to the optical axis are focused stronger than rays passing through outer areas of the lens at large numerical aperture (NA), which creates a larger focus in front of the main focus. Arrows in Fig. 4 c) numbered with 1 (small NA) and 2 (large NA) indicate the position of these foci. The tilting of the optics predominantly in the horizontal plane introduces an additional aberration (coma), which distorts the wave field asymmetrically [cf. Fig. 4d)].

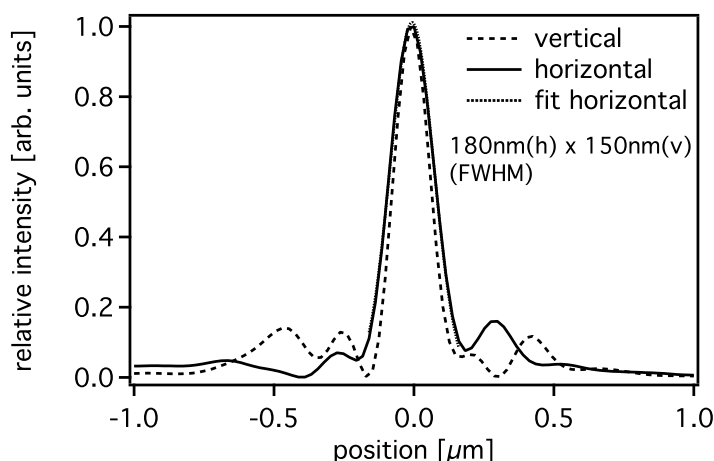


Figure 5. Intensity profiles extracted from the reconstructed wave field propagated into the main focal plane, showing a full-width-at-half-maximum (FWHM) focus size of 180 nm in horizontal and 150 nm in vertical direction, respectively.

In Fig. 5 intensity profiles extracted from the focal plane [arrow 2 in Fig. 4)] in horizontal and vertical direction are shown. The misalignment of the Be-CRLs in horizontal direction increases the Gaussian focus size to 180(h) × 150(v) nm² (FWHM).

5. CONCLUSIONS

We have shown that the characterization of XFEL nanobeams can be carried out fast and routinely using scanning coherent x-ray microscopy. The availability of fast detectors like the CSPAD allows one to collect a large set of diffraction patterns within minutes and, in combination with fast phase retrieval algorithms implemented on highly parallelizable graphics processing units (GPUs), nanobeam characterization based on ptychography can be accomplished in a very short time. The method will be especially important in all experimental scenarios where the precise knowledge of the illuminating wave field distribution is required for a quantitative analysis. The performance of the method is superior to standard imprint techniques. The latter only provides *postmortem* information on the intensity distribution and is often difficult to interpret. Especially in the presented case, where a slight misalignment of the optic creates a significant degradation of the focus quality and leads to an increase in spot size, the importance of an *in situ* beam characterization technique is emphasized. Ptychography yields the complete information on the nanofocused wave field with both high spatial resolution and dynamic range. It is applicable in all experimental environments providing enough space to guarantee the sampling requirements of coherent x-ray diffraction imaging. In the future a detector with smaller pixel size will be desirable, which allows one to either reduce the sample-detector distance or to investigate larger beams. Altogether, these improvements highlight the method's applicability as a real-time diagnostic for XFEL nanobeams.

ACKNOWLEDGMENTS

Portions of this research were carried out at the Linac Coherent Light Source (LCLS) at the SLAC National Accelerator Laboratory. LCLS is funded by the U.S. Department of Energy's Office of Basic Energy Sciences. The MEC instrument was supported by U.S. Department of Energy, Office of Fusion Energy Sciences. This work was funded by Volkswagen Foundation, the DFG under grant SCHR 1137/1-1, the Swedish Research Council and the Göran Gustafsson Foundation. The authors thank the MEC team, the detector group at SLAC providing us with the newest generation of the CSPAD, collaborating institutions as well as Bruno Lengeler for fruitful discussions and providing the CRL optics.

REFERENCES

- [1] Chapman, H. N., Barty, A., Bogan, M. J., Boutet, S., Frank, M., *et al.*, "Femtosecond diffractive imaging with a soft-x-ray free-electron laser," *Nature Physics* **2**(12), 839–843 (2006).
- [2] Chapman, H. N., Fromme, P., Barty, A., White, T. A., Kirian, R. A., *et al.*, "Femtosecond x-ray protein nanocrystallography," *Nature* **470**, 73–U81 (2011).
- [3] Vinko, S. M., Ciricosta, O., Cho, B. I., Engelhorn, K., Chung, H. K., *et al.*, "Creation and diagnosis of a solid-density plasma with an x-ray free-electron laser," *Nature* **482**, 59–62 (2012).
- [4] Glover, T. E., Fritz, D. M., Cammarata, M., Allison, T. K., Coh, S., *et al.*, "X-ray and optical wave mixing," *Nature* **488**, 603–608 (2012).
- [5] Chalupsky, J., Krzywinski, J., Juha, L., Hajkova, V., Cihelka, J., *et al.*, "Spot size characterization of focused non-Gaussian X-ray laser beams," *Optics Express* **18**(26), 27836–27845 (2010).
- [6] Hegerl, R. and Hoppe, W., "Dynamische Theorie der Kristallstrukturanalyse durch Elektronenbeugung im inhomogenen Primärstrahlwellenfeld," *Ber. Bunsen-Ges. Phys. Chem.* **74**, 1148 (1970).
- [7] Rodenburg, J. M. and Faulkner, H. M. L., "A phase retrieval algorithm for shifting illumination," *Appl. Phys. Lett.* **85**(20), 4795–4797 (2004).
- [8] Faulkner, H. M. L. and Rodenburg, J. M., "Movable aperture lensless transmission microscopy: A novel phase retrieval algorithm," *Phys. Rev. Lett.* **93**, 023903 (2004).
- [9] Schropp, A., Boye, P., Goldschmidt, A., Hönig, S., Hoppe, R., *et al.*, "Non-destructive and quantitative imaging of a nano-structured microchip by ptychographic hard x-ray scanning microscopy," *J. Microscopy* **241**(1), 9–12 (2011).
- [10] Bunk, O., Dierolf, M., Kynde, S., Johnson, I., Marti, O., *et al.*, "Influence of the overlap parameter on the convergence of the ptychographical iterative engine," *Ultramicroscopy* **108**(5), 481–487 (2008).
- [11] Thibault, P., Dierolf, M., Menzel, A., Bunk, O., David, C., *et al.*, "High-resolution scanning x-ray diffraction microscopy," *Science* **321**(5887), 379–382 (2008).
- [12] Thibault, P., Dierolf, M., Bunk, O., Menzel, A., and Pfeiffer, F., "Probe retrieval in ptychographic coherent diffractive imaging," *Ultramicroscopy* **109**(4), 338–343 (2009).
- [13] Schropp, A., Boye, P., Feldkamp, J. M., Hoppe, R., Patommel, J., *et al.*, "Hard x-ray nanobeam characterization by coherent diffraction microscopy," *Appl. Phys. Lett.* **96**(9), 091102 (2010).
- [14] Kewish, C. M., Thibault, P., Dierolf, M., Bunk, O., Menzel, A., *et al.*, "Ptychographic characterization of the wavefield in the focus of reflective hard X-ray optics," *Ultramicroscopy* **110**(4), 325–329 (2010).
- [15] Hönig, S., Hoppe, R., Patommel, J., Schropp, A., Stephan, S., *et al.*, "Full optical characterization of coherent x-ray nanobeams by ptychographic imaging," *Opt. Express* **19**(17), 16325–16329 (2011).
- [16] Vila-Comamala, J., Diaz, A., Guizar-Sicairos, M., Manton, A., Kewish, C. M., *et al.*, "Characterization of high-resolution diffractive x-ray optics by ptychographic coherent diffractive imaging," *Opt. Express* **19**(22), 21333–21344 (2011).
- [17] Hart, P., Boutet, S., Carini, G., Dubrovin, M., Duda, B., *et al.*, "The CSPAD megapixel x-ray camera at LCLS," *Proc. SPIE, X-Ray Free-Electron Lasers: Beam Diagnostics, Beamline Instrumentation, and Applications* **8504**, 85040C (2012).
- [18] Herrmann, S., Boutet, S., Duda, B., Fritz, D., Haller, G., *et al.*, "CSPAD-140k: A versatile detector for LCLS experiments," *Nuclear Instruments & Methods in Physics Research Section A* **718**, 550–553 (2013).

- [19] Miao, J., Charalambous, P., Kirz, J., and Sayre, D., “Extending the methodology of X-ray crystallography to allow imaging of micrometre-sized non-crystalline specimens,” *Nature* **400**, 342–344 (1999).
- [20] Schropp, A. and Schroer, C. G., “Dose requirements for resolving a given feature in an object by coherent x-ray diffraction imaging,” *New Journal of Physics* **12**, 035016 (2010).
- [21] Schropp, A., Hoppe, R., Patommel, J., Samberg, D., Seiboth, F., *et al.*, “Hard x-ray scanning microscopy with coherent radiation: Beyond the resolution of conventional x-ray microscopes,” *Appl. Phys. Lett.* **100**, 253112 (2012).
- [22] Fienup, J. R., “Phase retrieval algorithms: a comparison,” *Appl. Opt.* **21**(15), 2758 (1982).
- [23] Robinson, I. K., Vartanyants, I. A., Williams, G. J., Pfeifer, M. A., and Pitney, J. A., “Reconstruction of the shapes of gold nanocrystals using coherent X-ray diffraction,” *Phys. Rev. Lett.* **87**(19), 195505 (2001).
- [24] Williams, G. J., Pfeifer, M. A., Vartanyants, I. A., and Robinson, I. K., “Three-dimensional imaging of microstructure in Au nanocrystals,” *Phys. Rev. Lett.* **90**(17), 175501 (2003).
- [25] Shapiro, D., Thibault, P., Beetz, T., Elser, V., Howells, M., *et al.*, “Biological imaging by soft x-ray diffraction microscopy,” *P. Natl. Acad. Sci. USA* **102**, 15343–15346 (2005).
- [26] Robinson, I. K. and Miao, J., “Three-dimensional coherent x-ray diffraction microscopy,” *MRS Bulletin* **29**(3), 177–181 (2004).
- [27] Chapman, H. N., Barty, A., Marchesini, S., Noy, A., Hau-Riege, S. P., *et al.*, “High-resolution ab initio three-dimensional x-ray diffraction microscopy,” *J. Opt. Soc. Am. A* **23**, 1179–1200 (2006).
- [28] Pfeifer, M. A., Williams, G. J., Vartanyants, I. A., Harder, R., and Robinson, I. K., “Three-dimensional mapping of a deformation field inside a nanocrystal,” *Nature* **442**, 63–66 (2006).
- [29] Schroer, C. G., Boye, P., Feldkamp, J., Patommel, J., Schropp, A., *et al.*, “Coherent x-ray diffraction imaging with nanofocused illumination,” *Phys. Rev. Lett.* **101**(9), 090801 (2008).
- [30] Thibault, P. and Menzel, A., “Reconstructing state mixtures from diffraction measurements,” *Nature* **494**, 68–71 (2013).
- [31] Maiden, A. M. and Rodenburg, J. M., “An improved ptychographical phase retrieval algorithm for diffractive imaging,” *Ultramicroscopy* **109**(10), 1256–1262 (2009).
- [32] Schropp, A., Hoppe, R., Meier, V., Patommel, J., Seiboth, F., *et al.*, “Full spatial characterization of a nanofocused x-ray free-electron laser beam by ptychographic imaging,” *Scientific Reports* **3**, 1633 (2013).